

# Urban-Scale Building Air Change Rate Estimation Using Corrected Wind Speeds and Three-Zone Building Modeling

Yasemin Usta<sup>1</sup>, W. Stuart Dols<sup>2</sup>, Guglielmina Mutani<sup>1\*</sup>

<sup>1</sup> Department of Energy, Politecnico di Torino, Torino 10129, Italy

<sup>2</sup> National Institute of Standards and Technology, Gaithersburg, MD, 20899, USA

\*Email: [guglielmina.mutani@polito.it](mailto:guglielmina.mutani@polito.it)

Citation: Usta, Y., Dols, W.S., and Mutani, G. (2025). “Urban-Scale Building Air Change Rate Estimation Using Corrected Wind Speeds and Three-Zone Building Modeling,” *International Journal of Heat and Technology*, 45(5), pp. 1623–1630. Available at: <https://doi.org/10.18280/ijht.430501>.

## ABSTRACT

This study presents a scalable, time-efficient methodology for estimating building-specific air change rates by incorporating local urban morphology and wind conditions. The presented methodology is used to develop a QGIS-based plugin (Quantum Geographic Information System) to automate the integration of aerodynamic parameters derived from the Urban Multi-scale Environmental Predictor, with a simplified three-zone lumped-parameter model and multizone airflow simulations using CONTAM. The plugin calculates façade-specific wind-speed modifiers across 30° directional intervals. These modifiers are then used in a three-zone CONTAM model to calculate hourly building air change rates. The results were incorporated into an hourly energy consumption model for space heating and validated against measured energy use from residential buildings in Turin, Italy. Results show that replacing constant air change rates with site-specific estimates reduced the Mean Absolute Percentage Error by 11 % to 20 %. In particular, the error was reduced from 49 % ± 9 % to 32 % ± 6.5 % in January, corresponding to relative error reductions of approximately 34 %. The proposed method demonstrates improved accuracy in simulating building energy consumption considering the influence of an accurate shape of the urban environment on air change rates; moreover, it offers an automated framework for urban-scale assessments of ventilation, infiltration, and energy performance.

**Keywords:** Air Change Rate; Building Infiltration; Urban Roughness; UMEP; Multizone Airflow; Energy Modeling; QGIS Plugin

## 1. INTRODUCTION

Accurate estimation of building infiltration is essential for reliable energy performance assessments. However, most simulation tools mainly use constant air change rates (ACRs) based on construction period or archetype categories, overlooking both temporal variability and site-specific factors like urban roughness and local climate. This simplification can lead to significant errors in predicted infiltration rates and thus energy use and cost [1].

In urban environments, wind speed distributions are significantly affected by the presence and configuration of buildings, resulting in notable variations in wind velocities between inter-building spaces, urban canyons and rooftop levels compared to those observed in open, unobstructed areas. [2]. Context-specific Computational Fluid Dynamics (CFD) simulations can capture these effects, but their high computational requirements make them impractical for large-scale analyses [3, 4]. Instead, logarithmic wind-profile corrections adjust reference wind speeds at façade heights using two main aerodynamic parameters: displacement height ( $z_d$ ) and roughness length ( $z_0$ ).

Empirical methods, such as Kanda et al.’s study [5] of over 100 large-eddy simulations in Tokyo and Nagoya, link  $z_d$  and  $z_0$  to five geometric descriptors: mean and maximum building heights, plan area index (PAI), frontal area index (FAI), and building-height variability. This approach provides a practical way to estimate aerodynamic parameters with acceptable accuracy for urban scale analyses. Alternatively, the Urban Multi-scale Environmental Predictor (UMEP) [6, 7] plugin for QGIS (Quantum Geographic Information System) automates the derivation of these parameters across complex urban areas.

UMEP uses high-resolution 3D environment descriptions such as digital surface models (DSMs)—which capture terrain plus all above-ground features—and digital elevation models (DEMs)—which represent the bare-earth surface—along with land-cover data and building characteristics to compute associated morphometrics. These DSMs/DEMs, are typically derived from LiDAR or satellite sources [8], and can be imported directly into QGIS via GDAL tools or plugins [9]. UMEP then applies one of six roughness schemes (including Kanda’s) to calculate  $z_d$  and  $z_0$  for each wind-direction interval.

To apply wind corrections efficiently at the urban scale, building geometry must be simplified. In 2024, Santantonio et al. [10] introduced a three-zone lumped-parameter model that represents each building as two heated zones, upper and lower apartments, and an unheated shaft, enabling urban-scale simulations of combined wind-driven and buoyancy-driven infiltrations using corrected wind-speed inputs. Similarly, multizone tools like CONTAM can perform pressure-driven airflow simulations with leakage and weather inputs, but they depend on user-defined external boundary conditions that are typically input with limited consideration of the surrounding environment [11].

Given the need for site- and time-specific ACRs, a simplified workflow is essential. This study presents a QGIS-based methodology for wind-speed correction using UMEP derived aerodynamic parameters. The workflow automates the generation of building-specific wind-speed modifiers and integrates them into a three-zone CONTAM model.

By replacing fixed-value ACRs with dynamic, context-sensitive ACRs, this approach improves the accuracy of urban-scale energy assessments and provides more reliable ventilation and energy-use predictions.

In many energy performance assessment simulations, building ACRs are assumed constant — sometimes based on construction period or archetype, which can lead to substantial errors in heating and cooling load predictions. To address this limitation, this study presents an urban-scale methodology that automates calculations of hourly, site-specific building ACRs by integrating urban scale wind-speed corrections into a three-zone CONTAM model.

This methodology is used to develop a plugin within QGIS that mainly uses:

- UMEP derived aerodynamic parameters and wind-speed modifier calculations

Wind speed adjustments in urban canyons (highly obstructed areas) are determined based on the work by Georgakis and Santamouris [12], and Santamouris et al. [13], using the roughness length ( $z_0$ ), derived from UMEP simulations. Corrected wind speeds are then translated into wind-speed modifiers based on each building’s surrounding urban morphology.

- Three-zone building input parameters

Building attributes (height, number of floors, footprint area, envelope characteristics, and construction period) are used to create a detailed three-zone building database, which provides the necessary inputs for CONTAM simulations. A three-zone model is applied to each building based on the work by Santantonio et al. [10] and its accuracy is validated in the study by Usta et al. [14].

- Automated CONTAM simulations

For each building, CONTAM project files are generated automatically, and simulations are performed using a user-provided weather file to determine hourly building ACRs.

By employing dynamically computed, site-specific building ACRs, this methodology can improve energy consumption models at urban scale supporting energy cost-savings and ventilation strategies in high-density locations.

## 2. MATERIALS AND METHODS

Figure 1 illustrates the workflow for deriving site and time-specific building ACRs in urban environments, which is tested by using the resulting ACRs as inputs to an hourly energy consumption model. First,  $z_0$  is computed using UMEP for each wind direction considering an amplitude of  $30^\circ$ . Second,  $z_0$  is assigned to each building in the study area based on its location. Third, building-specific wind speed modifiers are calculated —accounting for location, orientation, and  $z_0$ — to generate a database containing properties of all buildings to be analyzed. Finally, this database is used to generate CONTAM project files for each building and to run hourly ACR simulations using a user-defined weather file. Moreover, the accuracy of the proposed methodology is measured comparing energy consumption models using the methodology presented by Mutani et al. [15] and three building ACR input scenarios: 1) fixed ACRs, 2) ACRs using the three-zone lumped-parameter model 3zLPM [10], and 3) using the building model of scenario 2 with UMEP-based real 3D urban environment wind speed correction presented in this paper. All three scenarios are compared with real measured hourly consumption data. The following subsections describe each of these steps in detail.

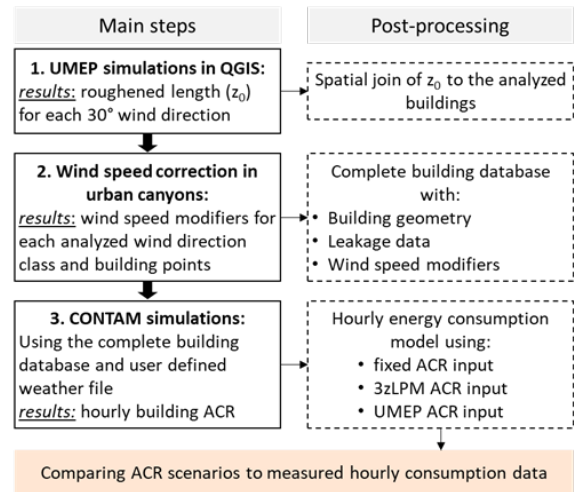


Figure 1. General methodology workflow

### 2.1 Aerodynamic parameter derivation with UMEP

The UMEP plugin requires several key inputs and settings to compute aerodynamic parameters (i.e.,  $z_0$ ) across the study area [6]:

- Analysis grid and search radius: A regular vector polygon grid defines the spatial resolution of the calculations. In this work, a 5 m by 5 m grid balances accuracy with computation time. A search radius of 200 m is used to aggregate surrounding morphometric parameters for each cell.
- Wind direction interval: In this work a  $30^\circ$  wind direction interval is used. Smaller intervals would improve directional resolution but increase processing time.
- 3D built environment representation: Acceptable spatial resolution for the DSM and DEM are required, along with a raster of above-ground objects (obtained by subtracting the DEM from the DSM). While higher resolutions capture buildings and vegetation more accurately but increase computational cost. In this work, a 1 m resolution is used for both DSM and DEM.
- Roughness calculation method: among UMEP’s six options, Kanda’s empirical scheme is selected for dense urban contexts. It relates the calculation of  $z_0$  to PAI, FAI, mean and maximum building heights, and building-height variability [5]. Using these inputs, UMEP computes  $z_0$  for each grid cell and wind direction interval, forming the basis for subsequent steps in the workflow.

### 2.2 Building database

The three-zone model assumes each building as a part of a continuous urban canyon (Figure 2(a)), thus this method is not applicable for detached buildings with four leakage sides. The representation of each single building (zones a, b, and c with leakage nodes 1 - 4) is illustrated in Figure 2(b). All geometric (volumes and node heights) and leakage parameters (leakage area of envelope and shaft doors) are derived from a polygon shapefile that contains each building’s height ( $H_{bld}$ ) and construction period. Building footprint area is calculated in QGIS using a Field Calculator expression, e.g.,  $\$area$ , to populate an “Area” field. All other building related data are calculated using the main parameters ( $H_{bld}$  and construction period), as provided in Table 1.

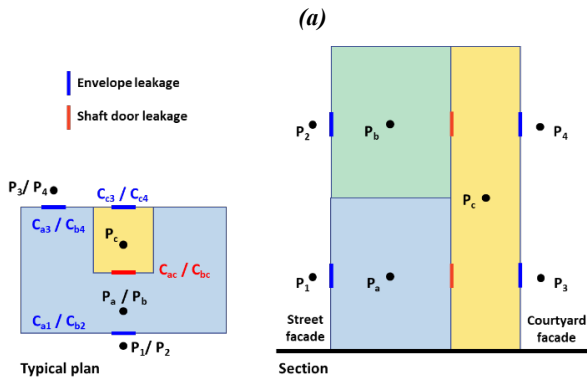
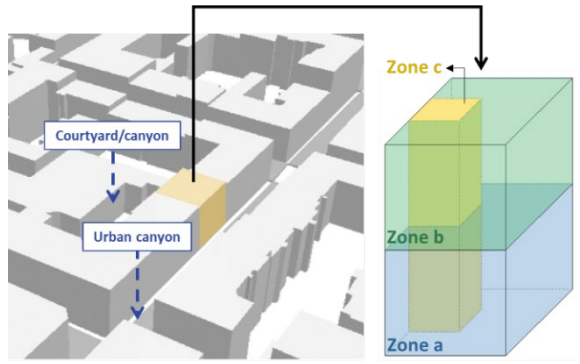


Figure 2. Three-zone building simplification

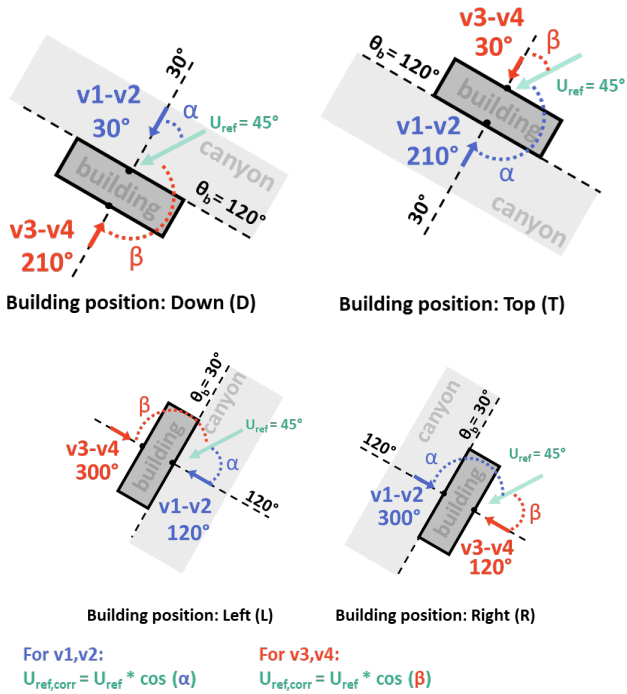


Figure 3. Building orientation ( $\theta_b$ ) and façade azimuth angle: canyon in blue, courtyard (or opposite) in red

Building orientation relative to the street network is determined by using QGIS's *Join by Nearest* tool to link building centroids to the closest street segment. The streets can be derived either by using the open street map within QGIS or from other available regional databases [16]. By comparing the x,y coordinates of each building centroid (on the ground plane) to its joined street segment, buildings are classified as Top (T), Down (D), Left (L), or Right (R). This in turn establishes the wall-azimuth angles for both the canyon façade and the opposite courtyard façade (Figure 3). These orientations enable façade-specific wind-speed corrections in

later steps ( $U_{ref,corr}$ ).

Table 1 summarizes the required main building database for both wind speed modifier calculation and for CONTAM simulations.

Table 1. Calculated building parameters for wind speed correction and airflow modeling

Variable	Formula / Method
Building Volume ( $V_{bld}$ ) [ $m^3$ ]	$V_{bld} = \text{Footprint Area} \times H_{bld}$
Shaft area ( $A_c$ ) [ $m^2$ ]	User-specified or estimated based on construction period
Shaft volume $V_c$ [ $m^3$ ] (lower: $V_{c1}$ and upper: $V_{c2}$ )	$V_c = \text{Shaft area} \times H_{bld}$ $V_{c1} = V_{c2} = V_c/2$
$V_a$ & $V_b$ [ $m^3$ ]	$V_a = V_b = (V_{bld} - V_c) / 2$
Level height for a and b ( $H_a$ and $H_b$ ) [m]	$H_a = 1/4 H_{bld}$ $H_b = 3/4 H_{bld}$
Leakage element height [m]	$H_{leakage} = H_a$ and $H_b$ in the middle of zone a and b heights
Roof height [m]	$H_{roof} = H_{bld}$
Shaft door multiplier per zone (represented in red in Figure 2 “ac-ca” & “bc-cb”)	$n_{doors} = (n_{floors} \times n_{apartments \text{ per floor}}) / 2$
Envelope and door leakage area (represented respectively in blue and red bold lines in Figure 2)	$A_{L,tot} = \text{wall/door area} \times A_L$ $A_L = \text{effective leakage area } cm^2/m^2 \text{ or } m^2/m^2$
Building orientation ( $\theta_b$ ) (see Figure 3)	Can be acquired from QGIS tool <i>Minimum Oriented Bounding Box</i>
Building position (top T, down D, left L, right R)	<i>Join By Nearest</i> tool between building polygon and street polygon
Canyon azimuth angle ( $\theta_{uc}$ ) [ $^\circ$ ]	$\theta_b \pm \beta$ , where $\beta = +90^\circ$ (L/T), $+270^\circ$ (R), $-90^\circ$ (D)
Courtyard azimuth angle ( $\theta_{co}$ ) [ $^\circ$ ]	$\theta_b \pm \beta$ , where $\beta = +270^\circ$ (L), $+90^\circ$ (R), $-90^\circ$ (T), $+90^\circ$ (D)
Canyon / courtyard width	From the street polygon

For example, zone height ( $H_a$ ,  $H_b$ ) refers to the level height required by CONTAM, which is half the building height for zone a and zone b. The airflow element height ( $H_{leakage}$ ) considered in the center of the zone levels (as illustrated previously in Figure 2). The shaft door multiplier is the number of doors per each link connecting zone a with c (through ac-ca) and zone b with c (through bc-cb) and is associated to the number of apartments per floor, which is then calculated based on the number of floors in the building. The typical leakage data ( $A_L$ ) required for the envelope leakage calculations is mainly related to building construction period and building materials. In this work, a leakage area of 2.642 per unit area [ $cm^2/m^2$ ] was used. Typical leakage data can be found in the study [17]. The total wall area, represented as an airflow element in Figure 2(b) (blue bold lines) is calculated using the geometrical attributes of the building calculated in earlier steps in QGIS.

With these building related data, each building record should contain all the fields required to generate façade-specific wind speed modifiers and to parameterize the three-zone airflow model for CONTAM.

## 2.3 Wind speed modifier calculations

Wind speed modifiers are required for CONTAM to correctly account for the wind pressure, which is significant driving force for air infiltration, on the analyzed façade points. Eq. (1) provides the wind pressure ( $P_w$ ) calculated in CONTAM.

$$P_w = \frac{\rho V_{met}^2}{2} C_h f(\theta) \quad (1)$$

where,

- $\rho$  is the ambient air density [ $\text{kg/m}^3$ ];
- $V_{met}$  is the wind speed measured at meteorological station [ $\text{m/s}$ ];
- $C_h$  is the wind speed modifier accounting for terrain and elevation effect [-];
- $f(\theta)$  is the coefficient that is a function of the relative wind direction. referred to as the wind pressure profile [-].

From Eq. (1), the term  $C_h f(\theta)$  links the wind direction to the façade azimuth angle (illustrated by the blue and red angles in Figure 3). CONTAM allows up to 16 angle/pressure coefficient pairs. These modifiers are calculated for each of the four façade points (1, 2, 3, and 4 in Figure 2(b)), across  $30^\circ$  wind direction intervals, ensuring that the directional variability of wind is accurately captured for each leakage point.

To derive these wind speed modifiers, the wind speed at each façade point is first corrected then it is used to obtain the modifier value for each point and angle. This process generates a set of wind speed modifiers for each building, tailored to its unique orientation and urban context. The following sections provide a detailed explanation of this calculation process.

### 2.3.1 Wind speed correction

Wind speed correction are computed following the approach by Georgakis et al. [12, 13], which applies two models based on the reference wind speed ( $U_{ref}$ ) from a weather station.

(1) When  $U_{ref} < 4 \text{ m/s}$  [13]:

Using a simple linear correlation method (Eq. (2)):

$$V_z = -0.537 + 0.957z/w - 0.012 \cdot \Delta T + 0.0039 \cdot U_{ref,corr} \quad (2)$$

where,

- $V_z$  is the corrected wind speed at height  $z$  [ $\text{m/s}$ ];
- $z$  is the height of the analyzed point [ $\text{m}$ ];
- $w$  is the width of the canyon or courtyard [ $\text{m}$ ];
- $\Delta T$  is the temperature difference between the ambient air and the canyon (or building envelope) surface temperatures at height  $z$  (in [15] can be calculated using: Eqq. 7, 8 and 9);

$U_{ref,corr}$  is the undisturbed wind speed corrected to account for the component perpendicular to the building façade [ $\text{m/s}$ ], as illustrated previously in Figure 3.

(2) When  $U_{ref} \geq 4 \text{ m/s}$  [12]:

$$V_{z,i} = U_{ref,corr} \cdot \log \left[ \frac{z+z_0}{z_0} \right] / \log \left[ \frac{z_{ref}+z_0}{z_0} \right] \quad (3)$$

where,

- $z_0$  is the roughness length derived from UMEP [ $\text{m}$ ];
- $z_{ref}$  is the height of the reference weather station [ $\text{m}$ ].

Thus, based on the hourly wind direction, the appropriate correction method is applied to compute wind speeds at points  $i = 1, 2, 3,$  and  $4$  (Figure 2).

### 2.3.2 Wind speed modifier

The modifiers  $M_{z,i} = (V_{z,i} / U_{ref})^2$  is calculated at each of the four points of each building for every hour.

### 2.3.3 Directional averaging

$M_{z,i}$  is then averaged within  $30^\circ$  intervals of wind direction and used to define wind pressure coefficient profiles for the CONTAM models of each building [18]. At the end of this step, the building database will include, in addition to the parameters discussed in Section 2.2, data pairs describing four wind speed coefficient profiles for building openings P1 – P4 where each profile consists of 12 angles ( $0^\circ, 30^\circ, 60^\circ \dots 330^\circ$ ) and modifier data points.

## 2.4 CONTAM input database and simulations

CONTAM simulates building airflow by solving a network of nodes (zones and duct junctions) connected by airflow paths (e.g., cracks, doorways, and duct segments) under the influence of driving forces — wind pressure, buoyancy (stack effect), and mechanical systems. To incorporate site specific wind effects, CONTAM requires as inputs:

- Weather File: A time series of outdoor parameters, i.e., ambient temperature [K], barometric pressure [Pa], wind speed [ $\text{m/s}$ ], and wind direction [ $^\circ$ ]. The weather file should be compatible with CONTAM (.wth) [19].
- Building zones and airflow connections: A description of each zone (e.g., lower and upper living zones, shaft) including their volumes, temperatures, and interconnectivity. Interzone airflow is defined by mathematical relationships between airflow and pressure, referred to as CONTAM airflow elements, e.g., *Leakage area* and *Large opening* elements.
- Leakage Areas: this power law model in CONTAM can be based on data from building pressurization tests, which measure airflow rates across pressure differences. For each flow coefficient (illustrated previously by blue and red bold lines in Figure 2), CONTAM requires the leakage area and test conditions, i.e., discharge coefficient ( $C_d$ ), flow exponent ( $n$ ), reference pressure difference ( $\Delta P$ ) [20]. Table 2 provides an example input data for Leakage Areas using the calculation method described by Usta et al. [14].

The complete building database generated in Section 2.3 serves as the base input for creating project files (.prj) for each analyzed building using CONTAM Factorial [21].

**Table 2.** Leakage area airflow element input in CONTAM

	Leakage characteristics	Unit	Value
Area	Per item	$\text{cm}^2$	By building geometry
	Per unit length	$\text{cm}^2/\text{m}$	
	Per unit area	$\text{cm}^2/\text{m}^2$	
Airflow reference conditions	Discharge coefficient, C	-	1
	Flow exponent, n	-	0.65
	Pressure difference	Pa	4

To enable batch simulation across an urban-scale building stock, a “flagged” project template was developed in

combination with a Python script. This script reads the building database — including geometry, leakage parameters, and wind speed modifiers — and inserts the relevant values into the template to produce modified .prj files. The script then executes CONTAM simulations for all buildings in the directory and aggregates the resulting hourly building ACRs into a single spreadsheet, indexed by building ID.

### 3. CASE STUDY

To demonstrate the applicability of the proposed methodology and the QGIS plugin, a set of residential buildings in Turin, Italy is selected. The buildings are chosen based on the availability of measured hourly energy consumption data and their location within census sections with different building densities. Table 3 provides the general characteristics of the selected 27 buildings, including their fixed ACR values and window-to-wall ratios (WWR) with respect to the construction period.

Table 3. General characteristics of the selected buildings

Construction period	ACR $h^{-1}$	WWR -	number of buildings
Before 1918	0.5	0.13	3
1919 - 1945			3
1946 - 1960		0.20	3
1961 - 1970			7
1971 - 1980			6
1981 - 1990	0.20	3	
1991 - 2000		1	
2013	0.3	0.20	1
Total			27

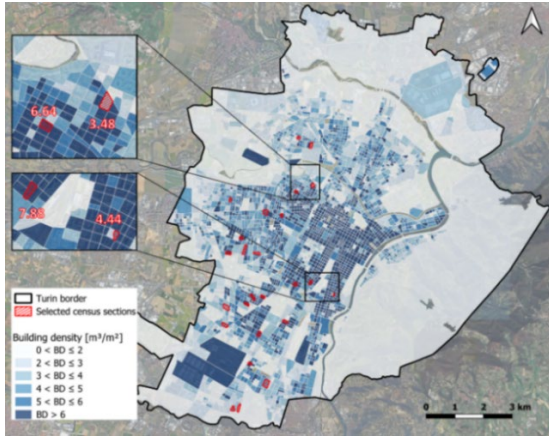


Figure 4. Building density for each census section in Turin

Figure 4 illustrates the spatial distribution of these case study buildings' location within Turin. Local meteorological inputs (outdoor temperature, wind speed, wind direction, and atmospheric pressure) were obtained from the Politecnico di Torino weather station [22].

### 4. RESULTS AND DISCUSSION

This section presents the results obtained from each stage of the proposed methodology, beginning with the wind speed correction using UMEP, followed by the calculation of wind speed modifiers and the simulation of building-specific ACRs using the three-zone CONTAM model. Finally, the performance of the model is evaluated by comparing the resulting hourly ACR-based energy consumption estimates

with real measured data under different ACR input scenarios.

#### 4.1 UMEP results for wind speed modifier calculations

UMEP simulations generated building-specific values of  $z_0$  for thirteen wind direction intervals at  $30^\circ$  interval across the study area. Figure 5 presents an illustrative example of  $z_0$  values assigned to a selected building for each wind direction interval; N =  $0^\circ$  or  $360^\circ$ , E =  $90^\circ$ , S =  $180^\circ$ , W =  $270^\circ$ . These direction-dependent  $z_0$  values were then mapped to each hour of the meteorological time series, based on the prevailing wind direction.

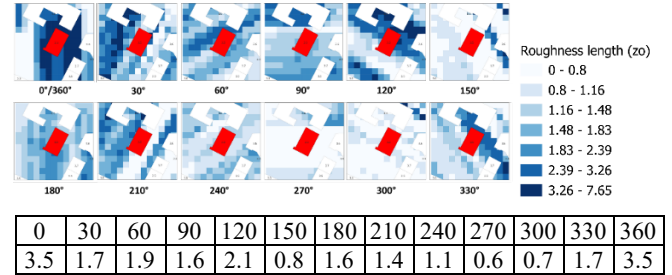


Figure 5. Roughness length ( $z_0$ ) maps for a sample building, with average  $z_0$  value assigned for each  $30^\circ$  wind direction

#### 4.2 Wind speed correction and wind speed modifier acquisition

Following the methodology outlined in Section 2.1 hourly façade-level wind speeds were computed at the four points on each building's façade (P1 - P4 in Figure 2). These calculations account for building-specific urban geometry, including the relative position of each point with respect to the prevailing wind direction and its height above ground.

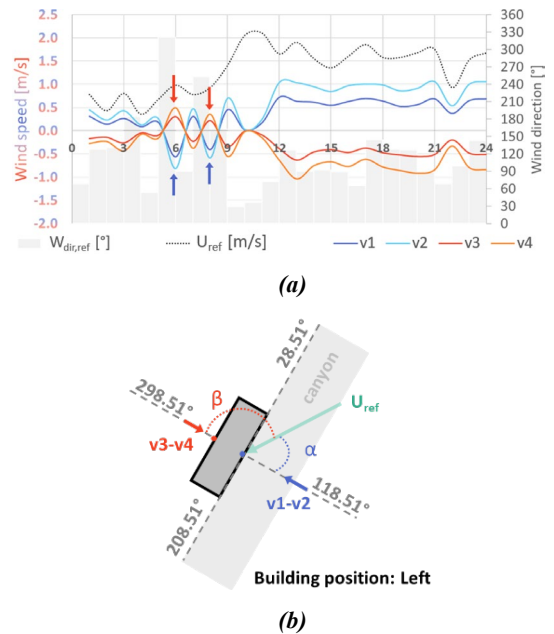


Figure 6. Hourly corrected wind speed at four façade points for a sample building, with the reference wind speed  $U_{ref}$  and direction  $W_{dir,ref}$

Figure 6 presents an example of corrected hourly wind speeds for four façade points for a sample building. The graphs clearly highlight the influence of wind direction and point height on wind speed magnitude and sign. In particular, by comparing Figure 6(a) and Figure 6(b), it can be observed that

the wind speed at points 1 and 2,  $v_1$  and  $v_2$ , (located on the street canyon façade and shown in blue) becomes negative — indicating leeward conditions — when the wind direction exceeds  $208.51^\circ$  or is below  $28.5^\circ$ . Furthermore, the reference wind speed (dotted line) shows significant reduction when the wind blows parallel to the canyon façade but remains relatively higher when the wind direction is close to perpendicular (between  $110^\circ$  and  $130^\circ$ ).

This process ensures that each façade point is assigned a wind speed value that accurately reflects its height and orientation, capturing the directional asymmetry of wind exposure and enabling the model to distinguish effectively between windward and leeward conditions.

Using these corrected wind speeds, wind speed modifiers were then calculated using  $M_{z,i} = (V_z / U_{ref})^2$ .

To align with CONTAM’s wind pressure input format, the hourly modifiers were averaged within each  $30^\circ$  wind direction interval (Figure 7) relative to the main façade (defined as  $0^\circ$ ). In this profile,  $0^\circ$  represents wind blowing perpendicularly toward the façade,  $90^\circ$  indicates wind flowing parallel from the right, and  $270^\circ$  from the left;  $180^\circ$  is perpendicular away from the façade.

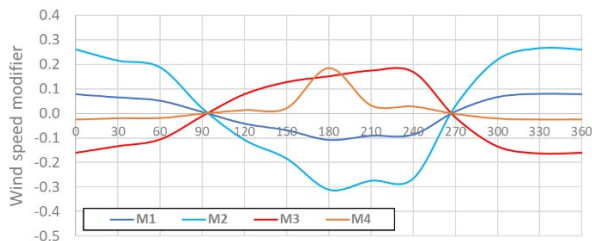


Figure 7. Wind speed coefficient profiles for four façade points as input for CONTAM

### 4.3 Hourly building ACR results

The hourly ACRs were calculated using the three-zone CONTAM model, incorporating the building-specific database developed in earlier steps. This database includes geometric properties, leakage parameters, and wind speed modifiers tailored to each building’s local urban context. The simulations were performed for all 27 buildings using CONTAM Factorial and the automated Python script for batch processing, achieving an elapsed simulation time of 13 seconds. This efficient workflow demonstrates the feasibility of applying the method to urban-scale analyses.

Figure 8 presents the hourly ACR profiles for four representative buildings, along with their respective volumes and surface-to-volume (S/V) ratios. The comparison reveals a consistent trend: buildings with higher S/V ratios resulted in higher ACRs. This is attributed to their relatively larger envelope area compared to the limited interior volumes. However, most residential buildings in Turin are compact with low S/V ratio, thus having low building ACRs [23].

The findings highlight the influence of building geometry on infiltration behavior, emphasizing the importance of volumetric scaling in airflow modeling. This geometric sensitivity further supports the application of the three-zone simplification used in this study, which has been previously validated against a detailed building model [14]. The comparison demonstrated that, despite the reduced level of detail, the simplified approach provides overall acceptable accuracy for buildings up to 16 floors ( $\approx 52$  m) while improving computational efficiency.

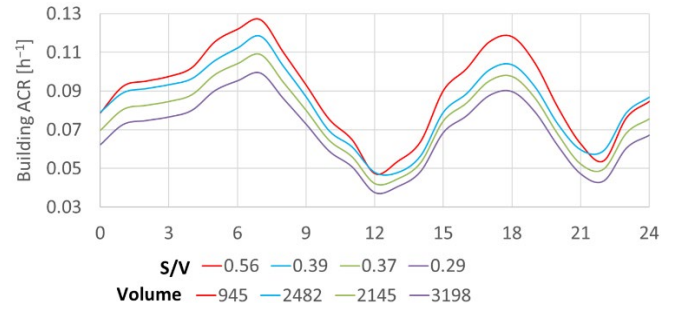


Figure 8. Hourly building ACR for four selected buildings with their volume and S/V values

### 4.4 Hourly energy consumption results

The hourly ACRs generated in the previous step — simulated using the three-zone CONTAM model with wind speed modifiers derived from UMEP — were used as input for a process-driven, hourly energy consumption model [15]. Such urban scale energy models propose a promising approach also for the analyses for future expansion of district heating network [24]. To assess the impact of this context-sensitive approach, the results of the energy consumption model using UMEP based ACRs were compared against two other ACR scenarios. The first scenario is using a fixed ACR based on the construction period of the building, the second scenario is ACR based on wind speeds corrected within the urban canyon via CFD simulations using a three-zone lumped parameter model (3zLPM) [10].

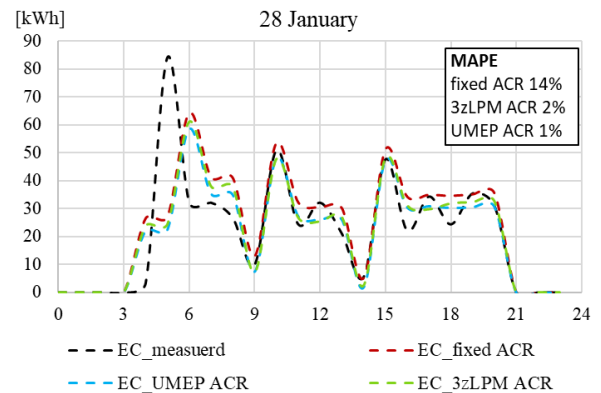


Figure 9. Hourly energy consumption (EC) using the three ACR scenarios and the measured data

All three scenarios were validated against measured hourly energy consumption data. Figure 9 illustrates the comparison of hourly energy consumption (EC) [kWh] for a representative day during the heating season using the three different ACR input scenarios. While the general trends in energy consumption are close, the daily Mean Absolute Percentage Error (MAPE) provided on the figure highlight the improvement in energy consumption calculations for both 3zLPM and UMEP ACR scenarios. Given inherent uncertainties in energy consumption measurement and modeling, daily-based MAPE and confidence interval (CI)—ranges around the monthly expected to contain the true value 95 % of the time—provide realistic ranges on model performance. To better understand the results for the whole heating season, Table 3 and Table 4 provide more pronounced differences.

Table 4 presents the MAPE for each scenario across representative months of the heating season, while Table 4 provides MAPE for selected days to provide more detailed

insights. The results consistently show that dynamic ACR approaches—both UMEP-based and 3zLPM—outperform fixed ACR assumptions. Notably, the 3zLPM ACR scenario demonstrated slightly higher accuracy than UMEP ACR. This is likely due to the inclusion of CFD-derived adjustments in the 3zLPM, which better capture wind dynamics influenced by urban canyon geometry and façade irradiance effects. For February, the fixed-ACR MAPE is now  $34.8\% \pm 8.5\%$  (95 % CI) vs.  $20.4\% \pm 6.0\%$  (95 % CI), confirming a statistically significant improvement.

The daily MAPE results in Table 5 further highlight this trend, confirming that both dynamic ACR methods improve model performance, with 3zLPM offering a slight advantage in representing localized airflow effects more comprehensively.

**Table 4.** MAPE of monthly energy consumption estimates during the heating season for three ACR input scenarios

	<b>fixed ACR</b>	<b>3zLPM ACR</b>	<b>UMEP ACR</b>
<b>November</b>	$40.5\% \pm 9.4\%$	$28.9\% \pm 6.7\%$	$29.8\% \pm 6.7\%$
<b>December</b>	$67.9\% \pm 9.6\%$	$47.2\% \pm 7.5\%$	$47.9\% \pm 7.3\%$
<b>January</b>	$49.3\% \pm 9.0\%$	$31.8\% \pm 6.3\%$	$32.4\% \pm 6.5\%$
<b>February</b>	$34.8\% \pm 8.5\%$	$20.0\% \pm 5.7\%$	$20.4\% \pm 5.9\%$

**Table 5.** Daily MAPE comparison of space heating demand predictions for selected days for three ACR input scenarios

	<b>Fixed ACR</b>	<b>3Zlpm ACR</b>	<b>UMEP ACR</b>
<b>24 November</b>	27.5 %	8.5 %	10.2 %
<b>11 December</b>	34.1 %	18.4 %	18.8 %
<b>10 January</b>	19.8 %	4.4 %	4.8 %
<b>20 February</b>	30.9 %	4.8 %	7.0 %

Overall, the findings confirm that integrating dynamic, site-specific ACR values—reflecting each building’s unique urban context—substantially enhances the accuracy of simulated energy demand, reinforcing the value of this approach for detailed and context-aware urban energy modeling.

## CONCLUSIONS

This study presented a methodology to enhance the accuracy of building ACR estimations in urban energy modeling by incorporating localized wind speed corrections of UMEP and simulating infiltration using a three-zone CONTAM model. The approach integrates detailed urban morphology—captured with the roughness length  $z_0$ —into wind speed adjustments, enabling the calculation of time and façade-specific ACRs across a diverse building stock.

To evaluate the effectiveness of the method, simulations using dynamic, context-specific ACRs (UMEP ACR) were compared against both a baseline scenario using fixed ACRs derived from building construction period (fixed ACR) and a scenario based on a previously developed three-zone lumped parameter model using CFD-based wind effects (3zLPM ACR). The comparison focused on simulated hourly space heating demand and was validated using measured energy consumption data from 27 buildings in Turin, Italy.

The results clearly demonstrate that integrating UMEP-derived ACRs substantially improves model accuracy. Across four representative months of the heating season (Table 4), the UMEP ACR approach reduced MAPE from fixed ACR values of  $67.9\% \pm 9.6\%$  (December),  $49.3\% \pm 9\%$  (January), and  $34.8\% \pm 8.5\%$  (February) to  $47.9\% \pm 7.3\%$ ,  $32.4\% \pm 6.5\%$ , and  $20.4\% \pm 5.9\%$ , respectively—all based on daily-level analysis. The non-overlapping confidence intervals confirm statistically significant improvements. Notably, in December and January, the MAPE was reduced from 68 % and 49 % (fixed ACR) to 48 % and 32 % (UMEP ACR), respectively representing relative error reductions of approximately 29 % and 35 %.

Daily comparisons (Table 5) show even more detailed results. On selected days such as January 10 and February 20, MAPE decreased from 20 % and 31 % (fixed ACR) to just 5 % and 7 % (UMEP ACR), marking error reductions of up to 75 %. The results were also comparable to the 3zLPM ACR approach, with UMEP ACR yielding slightly lower accuracy. This discrepancy may be attributed to the relatively coarse spatial resolution of the UMEP ACR method, which uses a 5 m grid to derive  $z_0$  values. As a result, while UMEP incorporates hourly wind direction and façade-specific modifiers, it still represents a generalized approximation of urban form compared to the more canyon specific CFD simulations used in the 3zLPM approach.

Overall, the findings validate the proposed approach as a robust and scalable method for integrating wind-driven infiltration into urban energy models. By capturing the spatial and temporal variability of wind-driven infiltration, the method significantly enhances prediction accuracy, supporting the value of localized ACR modeling for urban energy planning and simulation efforts.

## REFERENCES

- [1] Happle, G., Fonseca, J.A., Schlueter, A. (2017). Effects of air infiltration modeling approaches in urban building energy demand forecasts. *Energy Procedia*, 122: 283-288. <https://doi.org/10.1016/j.egypro.2017.07.323>
- [2] Delmastro, C., Mutani, G., Schranz, L., Vicentini, G. (2015). The role of urban form and socio-economic variables for estimating the building energy savings potential at the urban scale. *International Journal of Heat and Technology*, 33(4): 91-100. <https://doi.org/10.18280/ijht.330412>
- [3] Xu, X., Gao, Z., Zhang, M. (2023). A review of simplified numerical approaches for fast urban airflow simulation. *Building and Environment*, 234: 110200. <https://doi.org/10.1016/j.buildenv.2023.110200>
- [4] Blocken, B. (2015). Computational Fluid Dynamics for urban physics: Importance, scales, possibilities, limitations and ten tips and tricks towards accurate and reliable simulations. *Building and environment*, 91: 219-245. <https://doi.org/10.1016/j.buildenv.2015.02.015>
- [5] Kanda, M., Inagaki, A., Miyamoto, T., Gryschka, M., Raasch, S. (2013). A new aerodynamic parametrization for real urban surfaces. *Boundary-layer meteorology*, 148(2): 357-377. <https://doi.org/10.1007/s10546-013-9818-x>
- [6] UMEP Manual — UMEP Manual documentation. <https://umep-docs.readthedocs.io/en/latest/>, accessed on Jan. 5, 2025.
- [7] UMEP — QGIS Python Plugins Repository. <https://plugins.qgis.org/plugins/UMEP/>, accessed on Jan. 5, 2025.
- [8] USGS Lidar Explorer Map. <https://apps.nationalmap.gov/lidar-explorer/#/>, accessed on July 20, 2025.
- [9] GDAL Tools Plugin. [https://api.qgis.org/qgisdata/QGIS-Documentation-1.8/live/html/en/docs/user\\_manual/plugins/plugins\\_gdaltools.html](https://api.qgis.org/qgisdata/QGIS-Documentation-1.8/live/html/en/docs/user_manual/plugins/plugins_gdaltools.html), accessed on July 20, 2025.
- [10] Santantonio, S., Dell'Edera, O., Moscoloni, C., Bertani, C., Bracco, G., Mutani, G. (2024). Wind-driven and buoyancy effects for modeling natural ventilation in buildings at urban scale. *Energy Efficiency*, 17(8): 95. <https://doi.org/10.1007/s12053-024-10266-1>
- [11] CONTAM Introduction. *NIST*, Mar. 2018. <https://www.nist.gov/el/energy-and-environment-division-73200/nist-multizone-modeling/software/contam>, accessed on Jan. 5, 2025.
- [12] Georgakis, C., Santamouris, M. (2008). On the estimation of wind speed in urban canyons for ventilation purposes—Part 1: Coupling between the undisturbed wind speed and the canyon wind. *Building and Environment*, 43(8): 1404-1410. <https://doi.org/10.1016/j.buildenv.2007.01.041>
- [13] Santamouris, M., Georgakis, C., Niachou, A. (2008). On the estimation of wind speed in urban canyons for ventilation purposes—Part 2: Using of data driven techniques to calculate the more probable wind speed in urban canyons for low ambient wind speeds. *Building and Environment*, 43(8): 1411-1418. <https://doi.org/10.1016/j.buildenv.2007.01.042>
- [14] Usta, Y., Ng, L., Santantonio, S., Mutani, G. (2025). Lumped-parameter models comparison for natural ventilation analyses in buildings at urban scale. *Energies*, 18(9): 2352. <https://doi.org/10.3390/en18092352>
- [15] Mutani, G., Todeschi, V., Beltramo, S. (2020). Energy consumption models at urban scale to measure energy resilience. *Sustainability*, 12(14): 5678. <https://doi.org/10.3390/su12145678>
- [16] Geoportale Piemonte. [https://www.geoportale.piemonte.it/geonetwork/srv/ita/catalog.search#/metadata/r\\_piemon:062f33a0-4824-4bc8-bece-f9f0b5fe5ada](https://www.geoportale.piemonte.it/geonetwork/srv/ita/catalog.search#/metadata/r_piemon:062f33a0-4824-4bc8-bece-f9f0b5fe5ada), accessed on Jan. 5, 2025.
- [17] RDH Building Science. Study of part 3 building airtightness - Resources. <https://www.rdh.com/resource/study-of-part-3-building-airtightness/>, accessed on Jan. 5, 2025.
- [18] Walker, I.S., Wilson, D.J. (1994). Practical methods for improving estimates of natural ventilation rates. <https://www.aivc.org/resource/practical-methods-improving-estimates-natural-ventilation-rates>, accessed on May 7, 2025.
- [19] CONTAM Weather File Creator 2.0. *NIST*, Mar. 2018. <https://www.nist.gov/el/energy-and-environment-division-73200/nist-multizone-modeling/software/contam-weather-file>, accessed on Jan. 5, 2025.
- [20] Dols, W.S., Polidoro, B. (2020). CONTAM user guide and program documentation version 3.4. National Institute of Standards and Technology, Gaithersburg, MD. <https://www.nist.gov/publications/contam-user-guide-and-program-documentation-version-34>, accessed on Jan. 5, 2025.
- [21] CONTAM parametric analysis utilities. *NIST*, Mar. 2023. <https://www.nist.gov/el/energy-and-environment-division-73200/nist-multizone-modeling/contam-parametric-analysis>, accessed on Jan. 5, 2025.
- [22] LivingLAB@polito.it - Ambiente esterno. <https://smartgreenbuilding.polito.it/monitoraggio/estern.o.asp>, accessed on July 20, 2025.
- [23] Mutani, G., Todeschi, V. (2017). Space heating models at urban scale for buildings in the city of Turin (Italy). *Energy Procedia*, 122: 841-846. <https://doi.org/10.1016/j.egypro.2017.07.445>
- [24] Guelpa, E., Mutani, G., Todeschi, V., Verda, V. (2017). A feasibility study on the potential expansion of the district heating network of Turin. *Energy Procedia* 122: 847-852. <https://doi.org/10.1016/j.egypro.2017.07.446>

## NOMENCLATURE

ACR	Air Change Rate [ $\text{h}^{-1}$ ]
$A_L$	Leakage area [ $\text{m}^2$ ]
CI	Confidence Interval
C	Flow coefficient [ $\text{m}^3/\text{h}\cdot\text{Pa}^n$ ]
$C_d$	Discharge coefficient [-]
n	Flow exponent [-]
$\Delta P$	Pressure difference [Pa]
$U_{\text{ref}}$	Undisturbed reference wind speed at reference height [m/s]
$U_{\text{ref,corr}}$	Corrected reference wind speed with respect to building façade orientation [m/s]
$V_z$	Perpendicular wind speed at height z [m/s]
$z_0$	Roughness length [m]
DSM	digital surface model
DEM	digital elevation model
S/V	Surface-to-Volume ratio [ $\text{m}^2/\text{m}^3$ ]
QGIS	Quantum Geographic Information System
UMEP	Urban Multi-scale Environmental Predictor
3zLPM	Three-zone Lumped Parameter Model
CFD	Computational Fluid Dynamics
$M_z$	Wind speed modifier at height z [-]
MAPE	Mean Absolute Percentage Error [%]
WWR	Window-to-Wall Ratio [-]